

Particle-Based Implicit Solvent Model for Biosimulations: Application to Proteins and Nucleic Acids Hydration

Nathalie Basdevant, Tap Ha-Duong,* and Daniel Borgis*

*Laboratoire Analyse et Modélisation pour la Biologie et l'Environnement – UMR
8587, Bâtiment Maupertuis, Université d'Evry-Val-d'Essonne, Bd François Mitterrand,
91025 Evry Cedex, France*

Received February 3, 2006

Abstract: In addition to the simulation of two proteins described previously, we report on the application of our recently developed particle-based implicit solvent model to the simulations of four nucleic acid molecules, the 17 bases anticodon hairpin of the Asp-tRNA, the decamer d(CCGCCGGCGG) in both A and B form, and the containing EcoRI restriction site dodecamer d(CGCGAATTCGCG). The solvent is represented by a fluid of Lennard-Jones polarizable pseudoparticles of molecular size, the induced dipoles of which are sensitive to the solute electric field but not to each other. When implemented in a molecular dynamics algorithm with the Amber94 force field, the model allows to simulate efficiently the conformational evolution of the nucleic acids, yielding stable three-dimensional structures in agreement with experiments and other simulations in explicit solvent. In the same run, it is also able to provide estimations of the electrostatic solvation free energy within short time windows which correlate well with the Poisson–Boltzmann calculations. In addition, the molecular aspect of the solvent model allows for the reproduction of the highly localized water molecules in the major or minor grooves of the nucleic acid double helices, despite the absence of explicit water hydrogen bonds.

Introduction

Long and stable molecular dynamics simulations of nucleic acids in explicit solvent, such as TIP3 or SPC models, allow nowadays to analyze in detail the role of water in the stabilization of their three-dimensional structures and in the recognition processes by ligands or proteins. Several simulations in the nanosecond range have emphasized the crucial long-lived hydration patterns in both the minor and major grooves of DNA and RNA helices.^{1–5} Other theoretical studies have confirmed the importance of water molecules at DNA or RNA-protein interfaces for the stability and/or the selectivity of such complexes.^{6–10} Only a few studies have been interested in quantitative results of energetics and electrostatics in these complexes (see, e.g., refs 11–15). In this respect, however, the computational cost of simulations

in explicit solvent makes it difficult to estimate solvation free energies, and explicit solvent models do not allow for the estimation of proteins solvation free energy accurately, even with nanosecond-long simulations, because of the protein landscape which causes a prohibitive solvent penetration time. One possible approach is to combine molecular mechanics (MM) and continuum models by applying implicit solvent methods, such as Poisson–Boltzmann (PB) or generalized Born (GB) – solvent accessible surface area (SA) calculations, to structural snapshots extracted from MD simulations in explicit solvent.^{16–18} It should be noticed that this method has some connections to the earlier PDL/D/S-LRA method of Warshel and collaborators (semimicroscopic protein dipoles Langevin dipoles/linear response approximation),¹⁹ which has the merit to take additionally into account the protein reorganization effect. These so-called MM-PBSA or MM-GBSA calculations allow for relating molecules conformational changes to their free energy

* Corresponding author e-mail: daniel.borgis@univ-evry.fr (D.B.) and thaduong@univ-evry.fr (T.H.-D.).

variations and understand in detail the physical factors that favor or disfavor the stability and specificity of biomolecular systems. To avoid to generate computationally expensive molecular trajectories in explicit solvent, the GBSA solvent model can be implemented directly in an MD algorithm in order to provide in the same calculation both stable dynamics simulations and reliable solvation free energy estimations.^{20–22} This all-implicit solvation approach is much faster than the former MM-GBSA combination, but it neglects the molecular aspect of solvent, and it is therefore unable to provide structural information about the macromolecule first solvation shells that can be related or compared to observations from NMR or X-ray experiments.

We propose here an alternative solvent model that combines advantages of both explicit solvent (molecular aspect for structural information) and implicit solvent (efficient and rapid evaluation of solvation free energy). This model, which theoretical foundations are summarized in the first section, considers each solvent molecule as a Lennard-Jones particle that embeds a polarizable electric dipole (polarizable pseudoparticles or PPP model). The polarization of solvent dipoles obeys the macroscopic electrostatic laws of dielectric materials and provides a simple expression of the electrostatic solvation free energy. It should be noted that other promising methods tend to combine an efficient evaluation of solvation free energies with a characterization of the averaged solvation structure at a molecular level. Among these models, one should mention the density functional theory (DFT) approach that describes the aqueous environment around a solute in terms of both molecular density and polarization density^{23–25} and the three-dimensional integral equation theory which is able to provide averaged positional and orientational distribution function of the water molecules around a solute.^{26–28} The practicability and accuracy of these elaborated methods have been shown for various compounds in solution, but they still seem computationally too expensive for long molecular dynamics simulations of large biomolecules. As it will be shown in the methodology section, our original hydration model can be seen essentially as a particular DFT formulation for the solvent polarization density but projected on moving particles instead of fixed grid points. It can also be related to the iterative and noniterative grid-based Langevin dipole (LD) model,^{29–31} the surface constrained soft sphere dipoles model of Warshel,³² and to the more general class of dipolar solvent models.^{23–25,33–37}

Our solvent model has already been parametrized, tested, and applied to small peptides and proteins with satisfactory results, particularly in terms of CPU gain, since our model is about 5-fold faster than an explicit solvent model for simulations of solutes with around 1000 atoms.^{38,39} It can provide stable MD trajectories in the nanosecond range, yielding averaged structures in accordance with experimental observations as well as reasonable estimations of solvent electrostatic free energies with good correlations with Poisson–Boltzmann calculations.³⁹ In this paper, we report the results and analyses of nanoseconds long and stable molecular dynamics simulations of four nucleic acids molecules dissolved in our PPP semi-implicit solvent model. Trajec-

tories obtained in our previous work for two proteins, the bovine pancreatic trypsin inhibitor (5pti) and the B1 immunoglobulin-binding domain of streptococcal protein (1pgb), will be analyzed too for a broader perspective.

Methodology

Summary of the PPP Solvent Model. According to a macroscopic electrostatic theory, as formulated by Marcus,³³ when a solute built up with atomic point charges is immersed in a dielectric medium, a nonequilibrium electrostatic solvation free energy functional can be written as

$$\Delta F_{\text{pol}} = \int \frac{\mathbf{P}^2}{2\epsilon_0(\epsilon - 1)} dv - \int \mathbf{P} \cdot \mathbf{E}_0 dv - \frac{1}{2} \int \mathbf{P} \cdot \mathbf{E}_p dv \quad (1)$$

where ϵ_0 is the vacuum permittivity and ϵ is the solvent dielectric constant, \mathbf{P} is the nonequilibrium polarization density vector in a solvent elementary volume dv , \mathbf{E}_0 is the vacuum electrostatic field created by the solute atoms, and \mathbf{E}_p denotes the polarization electric field created by the polar medium surrounding the volume dv . The first integral is the free energy necessary to polarize the solvent volume dv . The second and third integrals account for the solute–solvent and solvent–solvent electrostatic interactions, respectively. Introducing into the Marcus functional the so-called “Coulomb field” or “local” approximation,^{40,37} which assumes that the polarization field remains longitudinal, yields the simplified solvation free energy functional:³⁵

$$\Delta F_{\text{pol}} = \int \frac{\epsilon \mathbf{P}^2}{2\epsilon_0(\epsilon - 1)} dv - \int \mathbf{P} \cdot \mathbf{E}_0 dv \quad (2)$$

The local approximation has been tested carefully for the solvation free energy of different solutes of complex shape in comparison to the Poisson–Boltzmann model.³⁷ In the case considered here of nonpolarizable solutes, the correlation with respect to Poisson–Boltzmann calculations is good, with correlation coefficients very close to 1, but the slope of the correlation line departs slightly from 1. It was shown that the agreement can be greatly improved by defining a systematic renormalization of the solute atomic charges in order to increase slightly the local dipoles. This feature will arise later in the computational details and parametrization section.

To calculate numerically the two integrals involved in eq 2, one could classically discretize the solvent region with a regular grid and consider at each point a dipole $\mu_i = \mathbf{P} dv = \mathbf{P}/\rho$, where ρ is the grid density. Then the electrostatic solvation free energy can be evaluated as

$$\Delta F_{\text{pol}} = \sum_i \frac{\mu_i^2}{2\alpha} - \sum_i \mu_i \cdot \mathbf{E}_{0i} \quad (3)$$

where \mathbf{E}_{0i} is the vacuum electrostatic field created by the solute atoms at the dipole μ_i position. The constant α is defined as $\alpha = \epsilon_0(\epsilon - 1)/(\epsilon\rho)$. It should be noted that α arises as a microscopic polarizability constant that is related to the medium macroscopic dielectric constant ϵ , and, therefore, it includes both the electronic and orientational polarization. The electrostatic solvation free energy at thermodynamic

equilibrium is obtained by minimizing ΔF_{pol} relative to all the μ_i which yields the following two simple expressions:

$$\mu_i^{\text{eq}} = \alpha \mathbf{E}_{0i} \quad (4)$$

$$\Delta F_{\text{pol}}^{\text{eq}} = -\frac{1}{2} \sum_i \mu_i^{\text{eq}} \cdot \mathbf{E}_{0i} \quad (5)$$

At this point, using eqs 4 and 5, the central idea of our method is to consider that the punctual dipoles μ_i^{eq} , are carried by discrete and mobile Lennard-Jones particles of molecular size, instead of the fixed nodes of a regular grid. Two particular features arising from our model should be emphasized: First, due to the local approximation, the induced dipoles do not interact with each other, and only Lennard-Jones interactions between solvent particles have to be calculated. Second, since the solvent pseudoparticles have translational degrees of freedom, the electrostatic solvation free energy $\Delta F_{\text{pol}}^{\text{eq}}$ calculated from eq 5 is in fact an “instantaneous” polarization free energy that has to be averaged over different particles positions, generated for example by molecular dynamics simulations. In practice, the electrostatic solvation free energy $\Delta F_{\text{pol}}^{\text{eq}}$ is included in the total Hamiltonian of the system, yielding the following expression:

$$H = K + V_{\text{Bond}}(\{\mathbf{R}_k\}) + V_{\text{Lj+Coul}}(\{\mathbf{R}_k\}) + V_{\text{Lj}}(\{\mathbf{r}_i\}) + V_{\text{Lj}}(\{\mathbf{R}_k - \mathbf{r}_i\}) + \Delta F_{\text{pol}}^{\text{eq}} \quad (6)$$

Here, K is the system kinetic energy, \mathbf{R}_k are the atomic positions of the solute, $V_{\text{Bond}}(\{\mathbf{R}_k\})$ denotes the solute bonded potential energy, including the stretching, bending, and torsion interactions, and $V_{\text{Lj+Coul}}(\{\mathbf{R}_k\})$ is nonbonded Lennard-Jones and Coulomb energy. The solvent pseudoparticles are characterized by a position \mathbf{r}_i and a solvent–solvent (possibly truncated) Lennard-Jones potential $V_{\text{Lj}}(\{\mathbf{r}_i\})$. The solute–solvent interactions are captured by the Lennard-Jones function $V_{\text{Lj}}(\{\mathbf{R}_k - \mathbf{r}_i\})$ and the electrostatic term $\Delta F_{\text{pol}}^{\text{eq}}$ described in eq 5. From the total potential energy of the system, the forces formulations are the same as in explicit models, except for the electrostatic solute–solvent forces which can be expressed in terms of partial derivatives of the vacuum electrostatic field \mathbf{E}_{0i} , on a solute atom (\mathbf{k}) and a solvent pseudoparticle (\mathbf{i}), respectively, by the following expressions:

$$\mathbf{F}_k = -\frac{\partial \Delta F_{\text{pol}}^{\text{eq}}}{\partial \mathbf{R}_k} = \sum_i \mu_i^{\text{eq}} \cdot \frac{\partial \mathbf{E}_{0i}}{\partial \mathbf{R}_k} \quad (7)$$

$$\mathbf{F}_i = -\frac{\partial \Delta F_{\text{pol}}^{\text{eq}}}{\partial \mathbf{r}_i} = \mu_i^{\text{eq}} \cdot \frac{\partial \mathbf{E}_{0i}}{\partial \mathbf{r}_i} \quad (8)$$

As shown in a previous paper, this solvation model leads to a potential of mean force for opposite charge ion pairs that is slightly too repulsive and without the expected two minima corresponding to the contact ion pair and the solvent separated ion pair.³⁸ This failure arises mainly from the local approximation, and in order to cure this deficiency, we have added another level of phenomenology to our solvation

model: We imposed that the solvent dipoles μ_i^{eq} can saturate when the electrostatic field \mathbf{E}_{0i} becomes too strong, instead of supposing a simple proportionality. As in the Langevin dipole model,³¹ this can be done by expressing the induced dipoles via a Langevin function

$$\vec{\mu}_i^{\text{eq}} = \frac{\mu_{\text{sat}}}{E_{0i}} L\left(3\alpha \frac{E_{0i}}{\mu_{\text{sat}}}\right) \mathbf{E}_{0i} \quad (9)$$

where $L(x) = \coth(x) - 1/x$, and μ_{sat} is the value of the dipoles saturation. Finally, to keep the simplicity of the solute–solvent electrostatic forces expressed in eqs 7 and 8, it has been demonstrated that the electrostatic solvation free energy $\Delta F_{\text{pol}}^{\text{eq}}$ has just to be reformulated as³⁸

$$\Delta F_{\text{pol}}^{\text{eq}} = -\frac{\mu_{\text{sat}}^2}{3\alpha} \sum_i \ln \left[\frac{\sinh\left(3\alpha \frac{E_{0i}}{\mu_{\text{sat}}}\right)}{\frac{E_{0i}}{3\alpha \mu_{\text{sat}}}} \right] \quad (10)$$

Computational Details and Parametrization. In this work, the force field used for nucleic acids molecules is the second generation Amber94 force field.⁴¹ As in our previous study on proteins,³⁹ the solvent pseudoparticles are characterized by the Lennard-Jones parameters $\sigma_{\text{LJ}} = 2.88 \text{ \AA}$ and $\epsilon_{\text{LJ}} = -3.197 \text{ kJ/mol}$ and a polarizability $\alpha = 2.33 \text{ \AA}^3$ calculated from the water dielectric constant $\epsilon = 80$ and a solvent density $\rho = 0.0337 \text{ \AA}^{-3}$. After trial and error, the value of the dipole saturation was fixed at an optimum value $\mu_{\text{sat}} = 1.5 \text{ D}$.

Since our solvent model is based on continuum electrostatics, we had to calibrate the atomic effective radii and partial charges in order to reproduce the known Born and Kirkwood electrostatic solvation free energies of isolated charged and neutral dipolar atoms. To fit to the Born solvation free energy,⁴² $\Delta G_{\text{Born}} = -1/2 (1-1/\epsilon)q^2/r$, we proceeded in the following way: For ions of different charge q and radius r , we first determined the solvation energy $\Delta F_{\text{pol}}^{\text{eq}}$ given by the PPP model, and we then reassigned to each of them an effective radius $r_{\text{eff}} = f_{\text{rd}} r$ where the rescaling factor is defined as $f_{\text{rd}} = \Delta G_{\text{Born}}/\Delta F_{\text{pol}}^{\text{eq}}$. For further studies with any force field, the atomic radii used for solute–solvent Lennard-Jones interactions have been rescaled systematically with the factor $f_{\text{rd}}(r_i, q_i)$.

As mentioned in our previous paper,³⁹ the local approximation in the PPP solvent model introduces a systematic error in the electrostatic solvation free energy of small neutral dipolar molecules. In the case of a point dipole μ embedded in a hard sphere of radius R and surrounded by a high dielectric material, one can show that the relative error with respect to the exact Kirkwood solvation free energy⁴³ $\Delta G_{\text{Kirkwood}} = -1/2(\epsilon - 1)/(\epsilon + 1/2)\mu^2/R^3$ amounts to 1/3. One way to correct these errors is to assign to the small molecules an effective dipole $\mu_{\text{eff}} = (3/2)^{1/2}\mu$ without changing their total charge. This can be done by rescaling the solute atomic partial charges q_i using the formula $q_i^{\text{eff}} = f_q q_i + (1 - f_q)Q_{\text{tot}}/N$, where Q_{tot} is the total charge of the small molecules, N is its number of atoms, and $f_q = (3/2)^{1/2}$

≈ 1.225 . It should be noted that the factor $f_q = 1.225$ which applies strictly to a spherical dipole with sharp boundaries should be slightly adjusted to accommodate for smooth and continuous Lennard-Jones boundaries. Numerous tests have led to the conclusion that the best results in terms of both structural stability and free energy correlations with Poisson–Boltzmann calculations are obtained with the factor $f_q = 1.185$.³⁹

Our solvation model has been implemented into the molecular dynamics program Orac⁴⁴ which uses a multiple time step r-RESPA algorithm.⁴⁵ In this work, three different time steps were used: a 4 fs time step for the integration of long-range nonbonded interactions (greater than 8 Å), a 2 fs time step for medium range nonbonded interactions (between 5 and 8 Å), and a 1 fs time step for short-range nonbonded (lower than 5 Å) and bonded interactions. The nonbonded interactions were smoothly cut with a switching function from 11 to 12 Å. All simulations were performed in the canonical NVT ensemble, using a Nosé–Hoover thermostat algorithm.^{46,47} All systems have been equilibrated progressively from 220 to 300 K during 228 ps and simulated at this last temperature for 4 ns without any constraints except those on bonds involving hydrogen, using the SHAKE algorithm.⁴⁸

Poisson–Boltzmann calculations of electrostatic solvation free energies of molecules were performed using the APBS software⁴⁹ with no ionic strength (explicit ions are included in the simulations) using a dielectric constant of $\epsilon_i = 1$ inside the solute and $\epsilon = 80$ outside and a solvent radius of 1.4 Å for probing the solute surface. The cubic grid for the finite differences algorithm of APBS was set to 141 nodes in each dimension for a rectangular box of the same size as the one used for the MD simulations, so that the grid size was below 0.5 Å.

Results

Stability of Proteins and Nucleic Acids Simulations. The PPP solvent model has been used previously to simulate two solvated proteins, the bovine pancreatic trypsin inhibitor (PDB code: 5pti) and the B1 immunoglobulin-binding domain of streptococcal protein G (1pgb). The 2-ns long production trajectories were proved stable and meaningful, with RMSD comparable to all-atom simulations and structural characteristics in overall agreement with X-rays and NMR measurements.³⁹

In this paper we substantiate our study with the structure, dynamics, and solvation properties of four different nucleic acid molecules. The starting structures were taken from the crystallographic structures available in the Nucleic Acid Database:⁵⁰ the 17 bases anticodon hairpin of the Asp-tRNA (trna05),⁵¹ the decamer d(CCGCCGGCGG) in both A form (adj109)⁵² and B form (bd0015),⁵³ and the containing EcoRI restriction site dodecamer d(CGCGAATTCGCG) (bdl001).⁵⁴ These four negatively charged molecules have been neutralized with an appropriate number of sodium counterions initially placed at 6 Å from the phosphate groups, except for bd0015 for which ions were placed at 3 Å. All the molecular systems considered, proteins and nucleic acids were simulated in a $48 \times 48 \times 70.7$ Å³ box, containing about

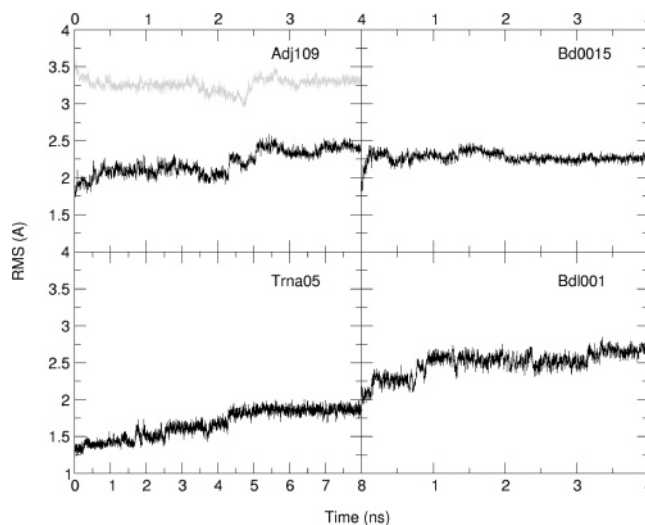


Figure 1. Time evolutions of the RMS deviation calculated over nucleic acids all non-hydrogen atoms from their initial structures (black lines). For the d(CCGCCGGCGG) decamer in A form, the RMS deviation from the B conformation is also plotted in gray line.

5200 solvent pseudoparticles. Molecular dynamics trajectories are 4-ns long for the three DNA molecules, whereas the trna05 trajectory was carried on for a total of 8 ns.

Figure 1 represents the RMS deviations (calculated over all non-hydrogen atoms) from the starting structures as a function of time for the four studied nucleic acids. This global structural criterion shows that all nucleic acid molecules are stable in a PPP solvent and remain close to their initial conformation during the 4 ns trajectories, the maximum RMS deviation being observed around 2.7 Å for the dodecamer bdl001, which is very close to the value obtained for a 5 ns MD simulation using a TIP3P water model.⁵⁵ The relatively small RMS deviation observed for the tRNA loop during the whole length of the 8-ns trajectory (around 1.9 Å at the end of the trajectory) is comparable to that obtained in a series of 3-ns long MD simulations performed in an explicit SPC/E solvent (1.7 Å on average) by Auffinger and Westhof.⁵⁶ It reveals that the tRNA structure is globally very stable with the PPP solvent, although it has been previously shown that this tRNA loop is particularly sensitive to the representation of solvent.⁵⁶ It reflects smaller deformations of RNA compared to DNA molecules, even in A form, for which the RMS deviation is stabilized around 2.5 Å. In Figure 1 is also plotted the RMS deviation of the decamer d(CCGCCGGCGG) in A form relative to the crystallographic B conformation. These two structures being initially distant by a RMSD of about 5.4 Å, it appears that the simulated A-DNA slightly drifts toward a B-like conformation, with a final RMSD around 3.3 Å away from the experimental B form. As it will be detailed below, this A to B partial transition, which is not observed for RNA, has been characterized by numerous molecular dynamics simulations on various DNA sequences with different force fields and water models.^{2,57–60}

The partial conclusion to be drawn here is that, as for proteins, the PPP solvent model allows for the reproduction of the global structural stability of different kinds of nucleic

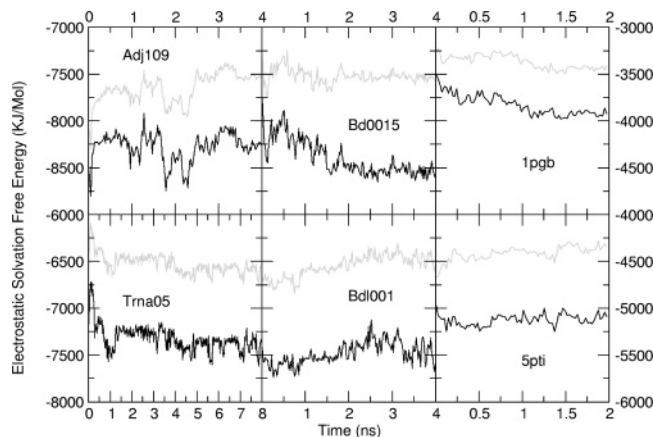


Figure 2. Time evolution of the nucleic acids and proteins electrostatic solvation free energies. Calculations with the PPP solvent model and with the Poisson–Boltzmann equation are plotted respectively with black lines and gray lines. For clarity and convenience, all plots have been translated into the same energy range.

acids molecules in comparison to available MD simulations using explicit solvent models.

Electrostatic Solvation Free Energies for Proteins and Nucleic Acids. As mentioned in the Introduction, the PPP solvent model provides an efficient way to estimate “on-the-fly” electrostatic solvation free energies during molecular dynamics simulations. Nevertheless, it should be mentioned that, whereas the solvent dipole orientations are in equilibrium at each simulation step, the pseudoparticles translational positions have to be sampled in order to yield an averaged solvation free energy corresponding to a real equilibrium state. Previous tests on small peptides have shown that these translational degrees of freedom are rapidly equilibrated within a few dozen picoseconds of simulation.³⁹ Thus, to compare the electrostatic solvation free energies estimated with the PPP model and by the Poisson–Boltzmann equation resolution, we have proceeded in the following way: Over time-windows of 12 ps, the average value of the PPP electrostatic solvation free energy was compared to the electrostatic solvation free energy calculated using the APBS software⁴⁹ to solve the Poisson–Boltzmann equation for an averaged molecular structure determined over the same time-window (see Methodology section).

In Figure 2 we have plotted the time evolution of the electrostatic solvation free energies calculated “on-the-fly” with the PPP solvent model and a-posteriori with the APBS algorithm. The figure includes the four nucleic acid molecules and the two proteins (5pti and 1pgb). These two charged proteins were simulated without neutralizing counterions and using a nonbonded interaction cutoff of 12 Å. Therefore, to account for the long-range solute–solvent electrostatic contribution of the solvation free energy (which is negligible for neutral solutes), we have added to the PPP solvation free energy a bulk correction evaluated by a continuum approximation using the Born formula $\Delta G_{\text{Bulk}} = -1/2(1-1/\epsilon)Q^2/R_{\text{Bulk}}$, where Q is the solute total charge and R_{Bulk} is the distance beyond which the solvent dipoles were supposed insensitive to the solute electrostatic field. In our simulations, the R_{Bulk} distance is physically defined as the

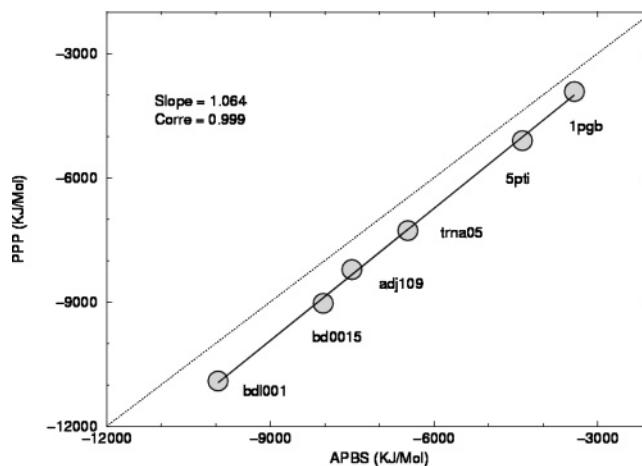


Figure 3. Comparison between the PPP and Poisson–Boltzmann electrostatic solvation free energies for the four nucleic acid molecules and the two proteins described in the text.

sum of the protein averaged gyration radius (about 14 Å for the two proteins) and the nonbonded interaction cutoff distance.

Despite the fact that we do not compare completely identical physical quantities (an average of free energies versus a free energy of an averaged structure), the plots in Figure 2 indicate visually that the variations of the PPP electrostatic solvation free energy due to the solutes conformational changes correlate well with those calculated with the Poisson–Boltzmann equation. Despite a systematic shift between the two values, correlation coefficients between the two methods range from 0.83 to 0.89 for nucleic acids (calculated over the last 2 ns of the trajectories) and from 0.76 to 0.86 for proteins³⁹ (calculated over the last 1.75 ns of the trajectories). This trend is particularly noteworthy for the A-DNA molecule which undergoes a significant conformational transition to a mixed A and B form. Similar good correlations have been previously observed for two small 10 residues peptides that undergo large conformational variations.³⁹ These encouraging results show that the PPP solvent model can efficiently reproduce “on-the-fly” the fine structure dependent solvation free energy of flexible solutes, at the expense of a relatively short time average over the translational degrees of freedom of the pseudoparticles.

We have summarized the applicability of our PPP model to the estimation of electrostatic free energies in Figure 3. There are displayed the averages over the 2 last ns of simulations of the PPP and APBS electrostatic solvation free energies (except for the proteins, for which averages were taken on the last equilibrated nanosecond of the trajectories). This plot reveals an excellent correlation between the two approaches for all studied biomolecules, the correlation coefficient and the slope of the linear relationship being equal to 0.99 and 1.06, respectively. Reminded that the PPP solvent model can be used for rapid and long molecular dynamics simulations, this result opens prospects for future studies focusing on the solvent influence on the DNA-protein or protein–protein association specificity, for which both the solutes deformation and dehydration process play a important role. For this purpose, however, further validation is needed,

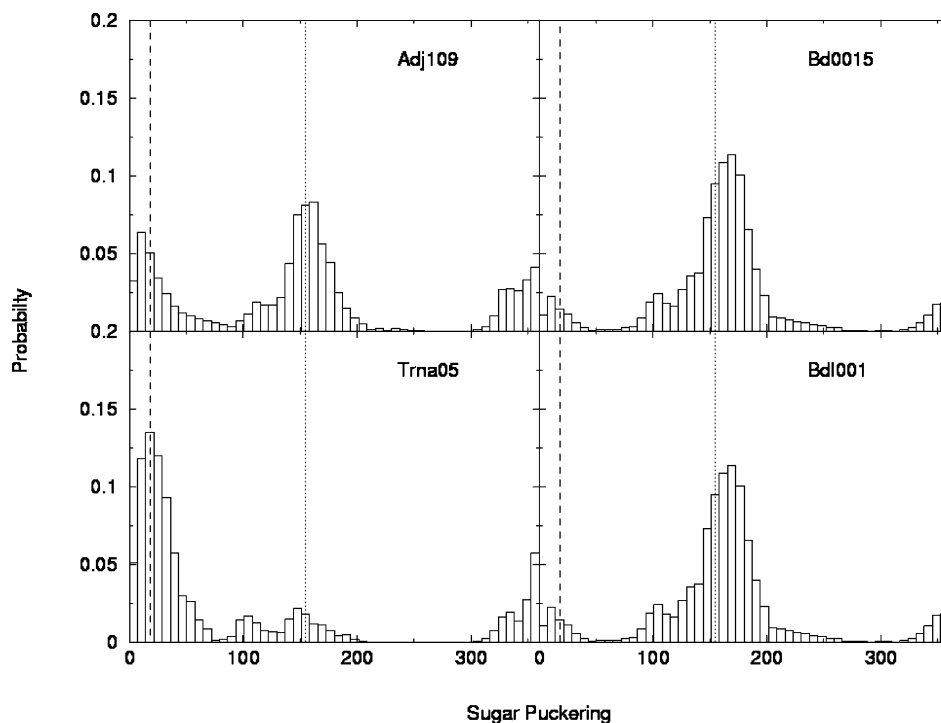


Figure 4. Probability distributions of the sugar pucker phases ($^{\circ}$) for the four studied nucleic acid molecules. The canonical values of the A- and B-DNA are represented respectively with dashed and dotted lines.

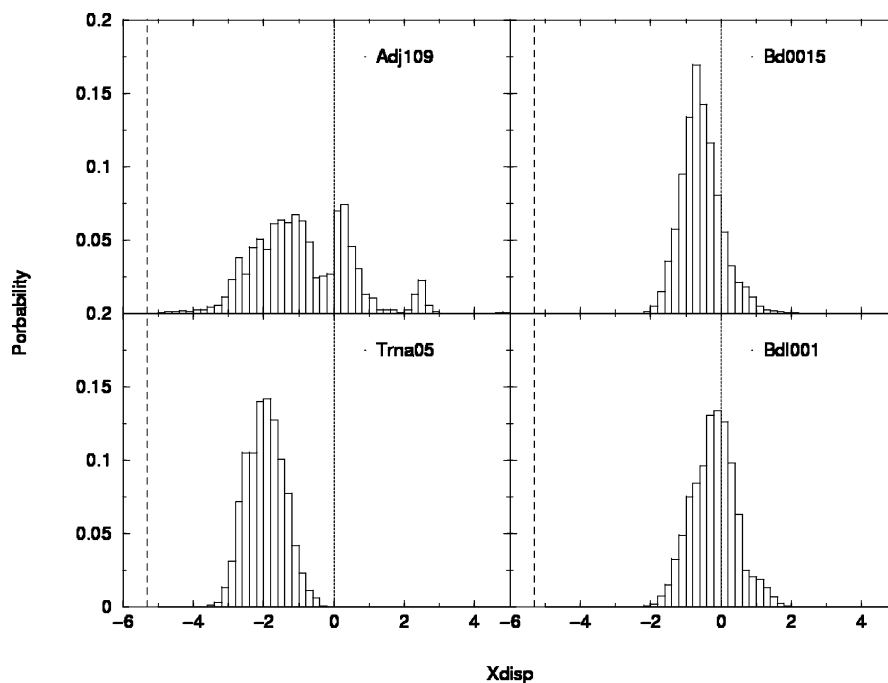


Figure 5. Probability distributions of the base pairs Xdisp (\AA) parameters, relative to the best curved helices axis.

like the prediction of mutational effects on protein–protein association⁶¹ or the comparison to experimental affinities. Provided this validation, the PPP solvent model can provide an efficient and self-consistent alternative to MM-PB or PDL/D/S-LRA calculations.

Structural Analysis of the Nucleic Acids. Since the structural properties of the proteins simulated in the PPP solvent were previously analyzed in details,³⁹ we focus here on the four nucleic acid molecules. We checked earlier in the paper the global stability of the molecules by looking at

time evolution of RMS deviations (see Figure 1), but more detailed analysis is needed in order to check the fine structure of nucleic acid molecules. We studied various helicoidal parameters of the DNA and RNA molecules, and we compared them with explicit simulations or experimental data. Various structural probability distributions pertinent to nucleic acids symmetries are displayed in Figures 4–7. These structural features were calculated on snapshots extracted every 12 ps from the 4 ns trajectories using the program CURVES (the first 4 ns in the case of trna05), which

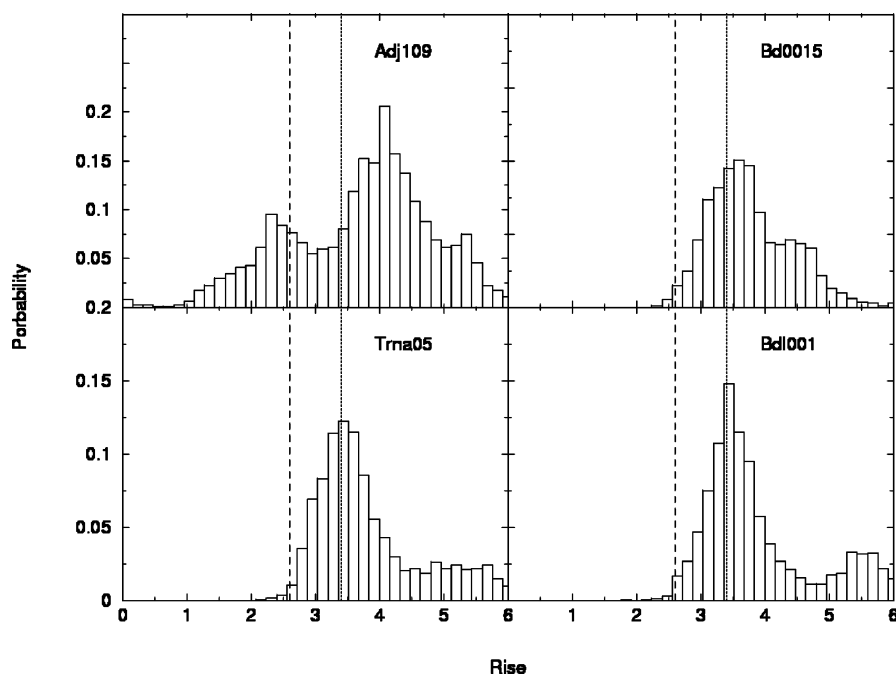


Figure 6. Probability distributions of the interbase pairs rise (Å) parameters.

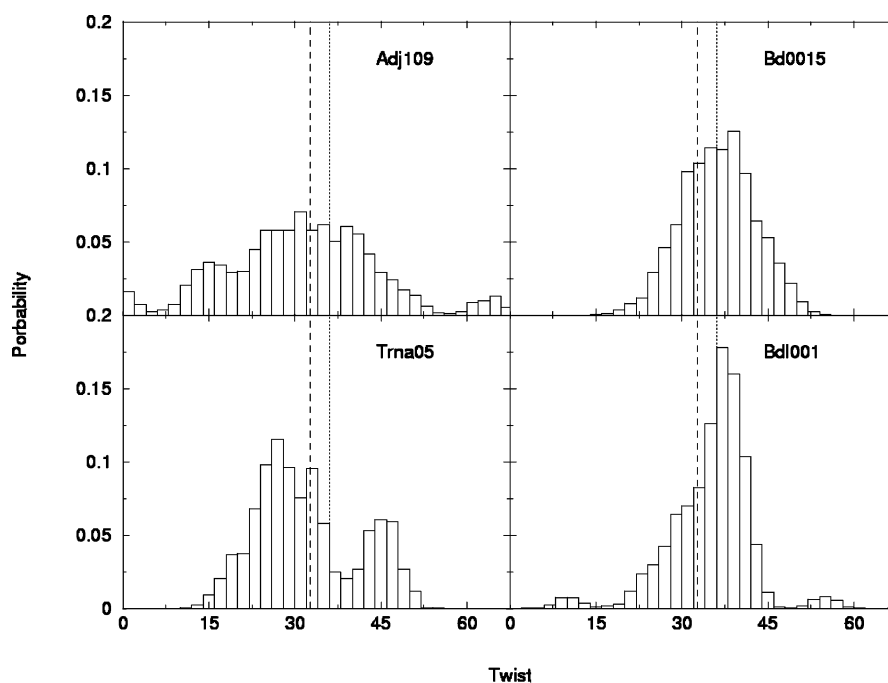


Figure 7. Probability distributions of the interbase pairs twist (°) parameters.

calculates the helicoidal parameters relative to an optimized nonlinear axis of the nucleic acid helices.⁶² Regarding the sugar pucker phase (Figure 4), the distribution peaks of the two B-DNA are close to the canonical *B* value, in the typical C2'-endo conformation. Moreover, as expected from canonical values of RNA molecules, the probability distribution of the tRNA has one maximum at the canonical *A* value, in the C3'-endo conformation. In contrast, the sugar pucker phase probability of the A-DNA decamer has clearly a bimodal distribution with one peak around the canonical *A* value, the other around the *B* one. This clearly reflects a partial transition of the molecule toward an intermediate structure between an *A* and a *B* conformation. This inter-

mediate structure is also confirmed by the probability distribution of the *Xdisp* parameter (Figure 5), which describes the displacement of the base pairs from the double helix axis. For the A-DNA, the *Xdisp* parameter also presents a bimodal distribution, whereas for the others nucleic acids, the distributions have only one maximum. This maximum is close to 0 Å, the canonical *B* value, for the two B-DNA, or has a negative value, characteristic of the A-form, for the tRNA molecule.

Figures 6 and 7 show the probability distributions of the rise and twist parameters, respectively, for the four studied nucleic acids helices. For the two B-DNA, the distributions are centered on the canonical *B* value. However, Figure 6

shows that the dodecamer bd1001 simulation yields some unusual high values of the rise parameter. A detailed analysis revealed that this is due to some incursions at intervals of two sodium ions between the base pairs C3/G4 and C9/G10 (data not shown). Similar incursions of counterions have also been observed between the two base pairs G3/C4 and G6/G7 of the A-DNA decamer adj109, for which the rise probability presents a bimodal distribution reflecting again a mixed form between A and B. The tRNA molecule simulation also yields high values of the rise parameter for the C3/G4 step (data not shown), but no incursion of counterions was observed in this case. This high rise is probably inherent to the presence of the wobble base pair G4-U14, which induces an unstacking and an underwinding of the RNA double helices as reviewed by Masquida and Westhof.⁶³ It should be noted that the rise parameters for the other tRNA base pairs are higher than the canonical A value, but they actually remain very close to the initial values of the crystallographic structure. The special geometry of the tRNA double helix due to the wobble base pair is also revealed by its twist parameter distribution (Figure 7), which shows a peak around 45° that arises from a high twist value for the G4/C5 step following the wobble pair. This overwound step is preceded by an underwound and high rise for the C3/G4 step, in agreement with experimental observations.⁶³ For both B-DNA molecules, as expected, the twist probability is sharply distributed around the canonical B value, whereas the A-DNA decamer distribution has a broad profile covering both the characteristic A and B values. Overall, despite some incursions of counterions between a few base pairs which can distort the double helices geometry at some intervals, the simulations of the four nucleic acids in the PPP solvent yield on average fine structures in good agreement with previous experimental and theoretical studies of the same molecules. This accomplishment should be stressed particularly for t-RNA, whose stability in silico was shown to be extremely sensitive to the solvent model employed, even in an explicit approach.⁵⁶

Nucleic Acids Hydration Sites. In contrast to a purely implicit solvent model such as the Poisson–Boltzmann equation or generalized Born, the PPP solvent is a particle-based model and thus keeps the molecular aspect of the solvent. Therefore, the PPP model allows for identifying the highly localized water molecules on the surface of biomolecules which are assumed to have a determinant structural influence upon their associations, as emphasized by NMR or crystallographic studies as well as MD simulations in explicit solvent.⁶⁴ The plots in Figures 8–10 represent a hydration index, the maximum residence time of a single solvent pseudoparticle close to different atom groups of the studied nucleic acids (defined in percentage with respect to the total simulation time). This quantity is similar to the “water residence time” usually measured or calculated from simulations. Since sodium counterions are able to occupy hydration sites, we have added to our “water residence time” the maximum residence time of sodium ions near the same sites. Three different groups of hydration sites were studied for each nucleic acid molecule: “Phosphate” hydration sites were considered as the four oxygen atoms bonded to the

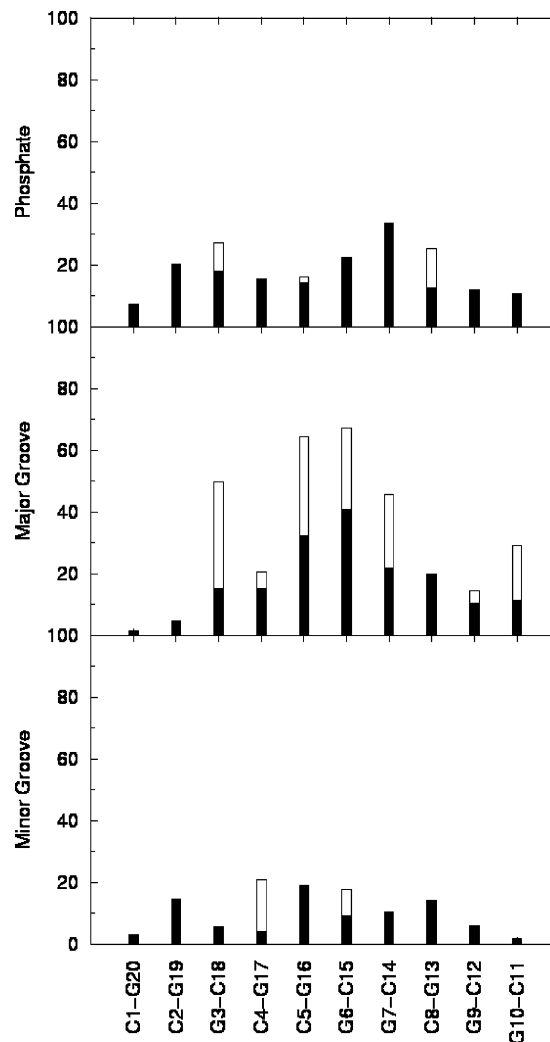


Figure 8. Maximum residence time (in % of the simulation length) of water molecules (black bars) and sodium ions (additional white bars) near the A-DNA d(CCGCCGGCGG) phosphate group, major groove and minor groove, as a function of the base pairs number.

phosphate atom. The “major groove” sites taken into account were the polar atoms N7 and O6 for guanine, the N7, N6, H61, and H62 atoms for adenine, the N4, H41, and H42 atoms for cytosine, and the O4 atom for thymine or uracil. The “minor groove” hydration sites were the N3, N2, H21, and H22 atoms for G, the N3 atom for A, and the O2 atom for C, T, or U. We specified that a solvent pseudoparticle or a sodium ion “occupies a hydration site” when its distance to a nitrogen or an oxygen site and to a hydrogen site were smaller than 3.0 and 2.5 Å, respectively. The results presented in Figures 8–10 are averages of the solvent and sodium maximum residence times over all the potential hydration sites for the three groups “phosphate”, “major groove”, and “minor groove” of each base (for tRNA) or base-pair (for all DNA molecules).

The first well-known result on nucleic acid hydration patterns that we reproduced is that the major grooves of A form double helices are more hydrated by the solvent pseudoparticles or sodium counterions than their minor grooves, whereas the longest water or ion residence times are found for the B-DNA minor groove rather than for the

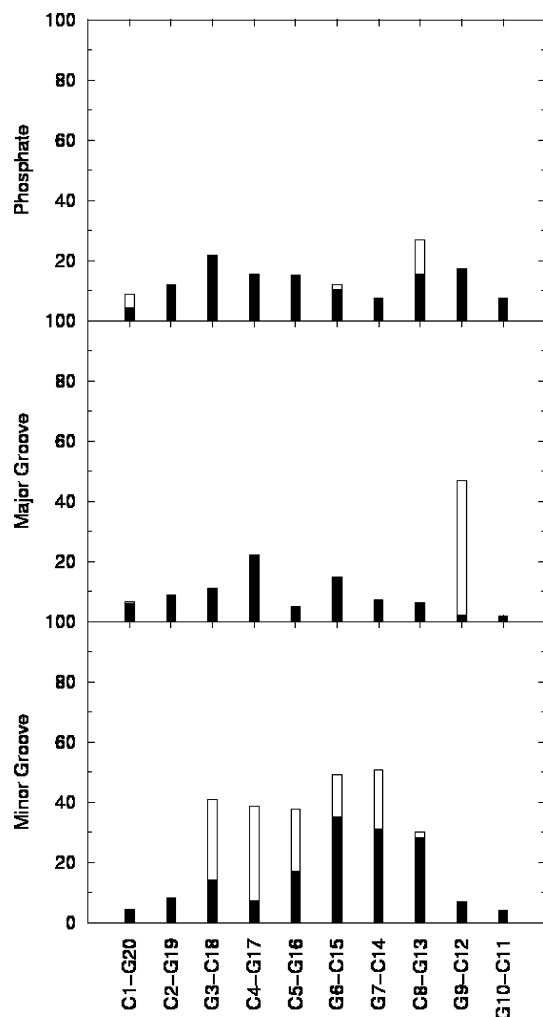


Figure 9. Solvent particles and ions maximum residence time for the B-DNA d(CCGCCGGCGG).

major one. Despite the absence of explicit hydrogen bonds, our solvent model allows for the reproduction of the preferential hydration sites on the nucleic acids double helix surfaces in general agreement with experimental observations.^{3,52,65–67} Concerning the decamer d(CCGCCGGCGG), it is remarkable in Figures 8 and 9 that several sodium counterions are highly localized into the major groove of the A conformation and into the B form minor groove, apparently replacing some long residency waters at these hydration sites. On the other hand, similar long-life sodium ions were not observed neither in the minor nor in the major groove of the B dodecamer d(CGCGAATTCGCG), especially in the AATT central region (data not shown). The presence of counterions in DNA minor groove and its sequence dependence is still theoretically unclear, especially by MD simulations, since the equilibration of ionic atmospheres around charged solutes in aqueous solvent turns out in the multnanoseconds range.^{1,2,4,55,68}

Similarly to the A-DNA, the double-helix part of the tRNA hairpin is preferentially hydrated (by PPP solvent molecules or ions) in the major groove, as shown in Figure 10. We found that the base pairs around the wobble G4-U14 pair are particularly well hydrated. This result is in agreement with previous results showing that the intrabase pair hydrogen

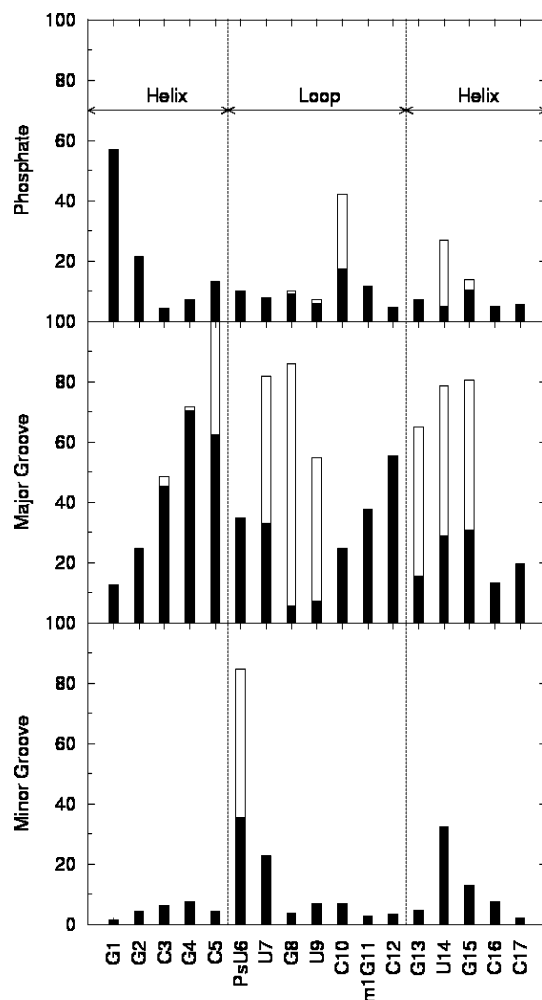


Figure 10. Solvent particles and ions maximum residence time for the tRNA-Asp anticodon hairpin.

bonds within the wobble pair are weak and more accessible to the solvent.⁶⁹ Our results show that the bases of the tRNA loop are preferentially bound to waters or ions in their major groove side, except for the pseudouridine (Ψ 6). In this case, the polar atoms of the base in the minor groove side appears to be better hydration sites, in agreement with the theoretical study of the same hairpin hydration by Auffinger and Westhof.⁶⁹ As these authors also noticed, the three anticodon bases GUC are not particularly hydrated by water molecules. However, in our simulation, this base triplet seems to be strongly bound to sodium counterions, which has not been observed previously in other simulations.

Despite the absence of explicit hydrogen bonds in the PPP solvent model, the general hydration patterns of nucleic acids previously determined by experiments or simulations in explicit solvent were correctly reproduced. The PPP model can thus provide some molecular information about hydration which is not accessible by classical implicit models such as generalized Born or Poisson–Boltzmann. One of the future challenges will be to obtain reliable energetic results for, e.g., nucleic acids/protein association and compare carefully with experimental data or available all-atom simulations.¹⁵

Computation Times. To conclude this study, we should recall the numerical performances of the PPP solvent model that have been previously presented.³⁹ We showed that, in

our present (not fully optimized) implementation, the CPU gain of the PPP solvent model with respect to a typical 3-sites explicit water model (TIP3) is around 12.5 for pure solvent and drops to about 5 for solutes of about 800 atoms (like tRNA, DNA, and 1pgb) surrounded by ~5000 solvent molecules. Moreover, the computational overhead of PPP compared to vacuum simulations is about 8 for a solute of more than 800 atoms (for which solute–solvent interactions and solute–solute interactions become comparable), which makes the PPP solvent model competitive with respect to, e.g., the most reliable implementations of the generalized Born model.

Conclusion

The polarizable pseudoparticle solvent model can be considered as the simplest possible particle-based model of a polar solvent. The particles induced dipoles do not see each other so that no self-consistent resolution is needed, and the solvent–solvent interactions are reduced to short-range (Lennard-Jones-like) interactions. When implemented in a molecular dynamics algorithm, this solvent model provides a fast and efficient way to simulate proteins and nucleic acids structures and dynamics as well as both the thermodynamic and structural aspects of their hydration. It makes it possible to reproduce the fine three-dimensional structures of biomolecules in agreement with experimental observations. For all studied biomolecules we observed a very good correlation between the electrostatic solvation free energy estimated with the PPP model and those accurately calculated with the Poisson–Boltzmann equation. This result allows for confidence for future investigations with the PPP model of the hydration influence on protein–protein or DNA–protein association specificity. Here, however, a careful comparison to experimental data and to available explicit water MD simulations results will be needed. Moreover, despite the absence of hydrogen bonds in the PPP solvent model, preferentially hydration sites of nucleic acids experimentally identified were correctly reproduced with our particle-based model, therefore adding some molecular information about hydration.

This study also reveals the unclear behavior of sodium counterions during the nucleic acids simulations due to their slow equilibration. To investigate more accurately the particular role of counterions in the structure and dynamics of highly charged solutes, an extension of our PPP model to include the ions implicitly in the model is currently ongoing. This will be done by adding on each solvent pseudoparticle a partial charge that will be determined at each MD step based on the minimization of a polarization and ionic density free energy functional equivalent to the Poisson–Boltzmann equation.

At the end, our PPP model can provide an interesting alternative to MM-PBSA, MM-GBSA, or PDL/D/S-SLRA calculations since the electrostatic free energies are estimated “on-the-fly”, as the MD trajectories of the system are propagated. The hydrophobic surface free-energy contribution can be easily evaluated on the fly too, using standard (and fast) algorithms. It could be also estimated by defining an average of the solvent particle density over short time

windows and an appropriate density free-energy functional. This approach is under study.

Acknowledgment. N.B. is supported by a grant from Genopole, which is gratefully acknowledged.

References

- (1) Feig, M.; Pettitt, M. *Biophys. J.* **1999**, *77*, 1769–1781.
- (2) Auffinger, P.; Westhof, E. *J. Mol. Biol.* **2000**, *300*, 1113–1131.
- (3) Stefl, R.; Koca, J. *J. Am. Chem. Soc.* **2000**, *122*, 5025–5033.
- (4) McConnell, K. J.; Beveridge, D. L. *J. Mol. Biol.* **2000**, *304*, 803–820.
- (5) Schneider, C.; Brandl, M.; Suhnel, J. *J. Mol. Biol.* **2001**, *305*, 659–667.
- (6) Sen, S.; Nilsson, L. *Biophys. J.* **1999**, *77*, 1782–1800.
- (7) Komeiji, Y.; Uebayasi, M. *Biophys. J.* **1999**, *77*, 123–138.
- (8) Tang, Y.; Nilsson, L. *Biophys. J.* **1999**, *77*, 1284–1305.
- (9) Tsui, V.; Radhakrishnan, I.; Wright, P. E.; Case, D. A. *J. Mol. Biol.* **2000**, *302*, 1101–1117.
- (10) Paulino, M.; Esperon, P.; Vega, M.; Scazzocchio, C.; Tapia, O. *J. Mol. Struct.* **2002**, *580*, 225–242.
- (11) Paillard, G.; Lavery, R. *Structure* **2004**, *12*, 113–122.
- (12) Lavery, R. *Q. Rev. Biophys.* **2006**, in press.
- (13) Florian, J.; Goodman, M. F.; Warshel, A. *J. Phys. Chem. B* **2000**, *104*, 10092–10099.
- (14) Florian, J.; Goodman, M. F.; Warshel, A. *J. Phys. Chem. B* **2002**, *106*, 5739–5753.
- (15) Florian, J.; Goodman, M. F.; Warshel, A. *Proc. Natl. Acad. Sci. U.S.A.* **2005**, *102*, 6819–6824.
- (16) Srinivasan, J.; Cheatham, T. E., III; Cieplak, P.; Kollman, P. A.; Case, D. A. *J. Am. Chem. Soc.* **1998**, *120*, 9401–9409.
- (17) Kollman, P. A.; Massova, I.; Reynes, C.; Kuhn, B.; Huo, S.; Chong, L.; Lee, M.; Lee, T.; Duan, Y.; Wang, W.; Donini, O.; Cieplak, P.; Srinivasan, J.; Case, D. A.; Cheatham, T. E., III *Acc. Chem. Res.* **2000**, *33*, 889–897.
- (18) Gohlke, H.; Kiel, C.; Case, D. A. *J. Mol. Biol.* **2003**, *330*, 891–913.
- (19) Muegge, I.; Tao, H.; Warshel, A. *Protein Eng.* **1998**, *10*, 1363–1372.
- (20) Bashford, D.; Case, D. A. *Annu. Rev. Phys. Chem.* **2000**, *51*, 129–152.
- (21) Tsui, V.; Case, D. A. *Biopolymers* **2001**, *56*, 275–291.
- (22) Calimet, N.; Schaefer, M.; Simonson, T. *Proteins* **2001**, *45*, 144–158.
- (23) Ramirez, R.; Gebauer, R.; Mareschal, M.; Borgis, D. *Phys. Rev. E* **2002**, *66*, 031206.
- (24) Ramirez, R.; Borgis, D. *J. Phys. Chem. B* **2005**, *109*, 6754–6763.
- (25) Ramirez, R.; Mareschal, M.; Borgis, D. *Chem. Phys.* **2005**, *319*, 261–272.
- (26) Pettitt, B. M.; Karplus, M.; Rossky, P. J. *J. Phys. Chem.* **1986**, *90*, 6335–6345.
- (27) Beglov, D.; Roux, B. *J. Phys. Chem. B* **1997**, *101*, 7821–7826.

- (28) Roux, B.; Simonson, T. *Biophys. Chem.* **1999**, *78*, 1–20.
- (29) Warshel, A.; Levitt, M. *J. Mol. Biol.* **1976**, *103*, 227–249.
- (30) Warshel, A.; Russel, S. T. *Q. Rev. Biophys.* **1984**, *17*, 283–422.
- (31) Florian, J.; Warshel, A. *J. Phys. Chem. B* **1997**, *101*, 5583–5595.
- (32) Warshel, A. *J. Phys. Chem.* **1979**, *83*, 1640–1652.
- (33) Marcus, R. A. *J. Chem. Phys.* **1956**, *24*, 979–989.
- (34) Pollock, E. L.; Alder, B. *J. Phys. A* **1980**, *102*, 1–21.
- (35) Calef, D. F.; Wolynes, P. G. *J. Phys. Chem.* **1983**, *87*, 3387–3399.
- (36) Frodl, P.; Dietrich, S. *Phys. Rev. A* **1992**, *45*, 7330–7354.
- (37) Borgis, D.; Levy, N.; Marchi, M. *J. Chem. Phys.* **2003**, *119*, 3516–3528.
- (38) Ha-Duong, T.; Phan, S.; Marchi, M.; Borgis, D. *J. Chem. Phys.* **2002**, *117*, 541–556.
- (39) Basdevant, N.; Borgis, D.; Ha-Duong, T. *J. Comput. Chem.* **2004**, *25*, 1015–1029.
- (40) Schaefer, M.; Karplus, M. *J. Phys. Chem.* **1996**, *100*, 1578–1599.
- (41) Cornell, W. D.; Cieplak, P.; Bayly, C. I.; Gould, I. R.; Merz, K. M., Jr.; Ferguson, D. M.; Spellmeyer, D. C.; Fox, T.; Caldwell, J. W.; Kollman, P. A. *J. Am. Chem. Soc.* **1995**, *117*, 5179–5197.
- (42) Born, M. *Z. Phys.* **1920**, *1*, 45–48.
- (43) Kirkwood, J. G. *J. Chem. Phys.* **1934**, *2*, 351–361.
- (44) Procacci, P.; Darden, T. A.; Paci, E.; Marchi, M. *J. Comput. Chem.* **1997**, *18*, 1848–1862.
- (45) Humphreys, D. D.; Friesner, R. A.; Berne, B. J. *J. Phys. Chem.* **1994**, *98*, 6885–6892.
- (46) Nosé, S. *J. Chem. Phys.* **1984**, *81*, 511–519.
- (47) Hoover, W. G. *Phys. Rev. A* **1985**, *31*, 1695–1697.
- (48) Ryckaert, J. P.; Ciccotti, G.; Berendsen, H. J. C. *J. Comput. Chem.* **1977**, *23*, 327–341.
- (49) Baker, N. A.; Sept, D.; Joseph, S.; Holst, M. J.; McCammon, J. A. *Proc. Natl. Acad. Sci. U.S.A.* **2001**, *98*, 10037–10041.
- (50) Berman, H. M.; Olson, W. K.; Beveridge, D. L.; Westbrook, J.; Gelbin, A.; Demeny, T.; Hsieh, S. H.; Srinivasan, A. R.; Schneider, B. *Biophys. J.* **1992**, *63*, 751–759.
- (51) Comarmond, M. B.; Giege, R.; Thierry, J. C.; Moras, D.; Fischer, J. *Acta Crystallogr. B* **1986**, *42*, 272–280.
- (52) Mayer-Jung, C.; Moras, D.; Timsit, Y. *Embo J.* **1998**, *17*, 2709–2718.
- (53) Timsit, Y.; Moras, D. *Embo J.* **1994**, *13*, 2737–2746.
- (54) Drew, H. R.; Wing, R. M.; Takano, T.; Broka, C.; Tanaka, S.; Itakura, K.; Dickerson, R. E. *Proc. Natl. Acad. Sci. U.S.A.* **1981**, *78*, 2179–2183.
- (55) Young, M. A.; Ravishanker, G.; Beveridge, D. L. *Biophys. J.* **1997**, *73*, 2313–2336.
- (56) Auffinger, P.; Westhof, E. *Biophys. J.* **1996**, *71*, 940–954.
- (57) Cheatham, T. E., III; Kollman, P. A. *J. Mol. Biol.* **1996**, *259*, 434–444.
- (58) Mackerell, A. D.; Banavali, N. K. *J. Comput. Chem.* **2000**, *21*, 105–120.
- (59) Trantirek, L.; Stefl, R.; Vorlickova, M.; Koca, J.; Sklenar, V.; Kypr, J. *J. Mol. Biol.* **2000**, *297*, 907–922.
- (60) Cheatham, T. E., III; Young, M. *Biopolymers* **2001**, *56*, 232–256.
- (61) Muegge, I.; Schweins, T.; Warshel, A. *Proteins* **1998**, *30*, 407–423.
- (62) Lavery, R.; Sklenar, H. *J. Biomol. Struct. Dynam.* **1988**, *6*, 63–91.
- (63) Masquida, B.; Westhof, E. *RNA* **2000**, *6*, 9–15.
- (64) Schwabe, J. W. R. *Curr. Opin. Struct. Biol.* **1997**, *7*, 126–134.
- (65) Shotton, M. W.; Pope, L. H.; Forsyth, T.; Langan, P.; Denny, R. C.; Giesen, U.; Dauvergne, M. T.; Fuller, W. *Biophys. Chem.* **1997**, *69*, 85–96.
- (66) Guerri, A.; Simpson, I. J.; Neidle, S. *Nucleic Acids Res.* **1998**, *26*, 2873–2878.
- (67) Makarov, V. A.; Pettitt, B. M.; Feig, M. *Acc. Chem. Res.* **2002**, *35*, 376–384.
- (68) Rueda, M.; Cubero, E.; Laughton, C. A.; Orozco, M. *Biophys. J.* **2004**, *87*, 800–811.
- (69) Auffinger, P.; Westhof, E. *J. Mol. Biol.* **1997**, *269*, 326–341.

CT0600417